

Stealth RF energy harvesting in MRI using selective shielding

Journal Article**Author(s):**

Bjorkqvist, Oskar; Pruessmann, Klaas P.

Publication date:

2024-07

Permanent link:

<https://doi.org/10.3929/ethz-b-000664974>

Rights / license:

[Creative Commons Attribution-NonCommercial-NoDerivatives 4.0 International](#)

Originally published in:

Magnetic Resonance in Medicine 92(1), <https://doi.org/10.1002/mrm.30048>

Funding acknowledgement:

181023 - Wireless Sensing and Real-Time Correction of Head Motion in MRI (SNF)

Stealth RF energy harvesting in MRI using selective shielding

Oskar Bjorkqvist¹ | Klaas P. Pruessmann²

Institute for Biomedical Engineering,
ETH Zurich and University of Zurich,
Zurich, Switzerland

Correspondence

Oskar Bjorkqvist, Institute for Biomedical Engineering, ETH Zurich and University of Zurich, Zurich, Switzerland.
Email: bjorkqvist@biomed.ee.ethz.ch

Funding information

Swiss National Science Foundation, BRIDGE Discovery, Grant/Award Number: 181023

Abstract

Purpose: To utilize the transmit radiofrequency (RF) field in MRI as a power source, near or within the field of view but without affecting image quality or safety.

Methods: Power harvesting is performed by RF induction in a resonant coil. Resulting RF field distortion in the subject is canceled by a selective shield that couples to the harvester while being transparent to the RF transmitter. Such shielding is designed with the help of electromagnetic simulation. A shielded harvester of 3 cm diameter is implemented, assessed on the bench, and tested in a 3T MRI system, recording power yield during typical scans.

Results: The concept of selective shielding is confirmed by simulation. Bench tests show effective power harvesting in the presence of the shield. In the MRI system, it is confirmed that selective shielding virtually eliminates RF perturbation. In scans with the harvester immediately adjacent to a phantom, up to 100 mW of average power are harvested without affecting image quality.

Conclusion: Selective shielding enables stealthy RF harvesting which can be used to supply wireless power to on-body devices during MRI.

KEYWORDS

RF harvesting, shielding, wireless power

1 | INTRODUCTION

Auxiliary in-bore and on-patient devices are receiving increasing interest in commercial MRI as well as MRI instrumentation research and could serve a range of purposes such as physiology monitoring, motion tracking or data transmission from receiver coils.^{1–3} Powering these kinds of devices via cable, as done traditionally, comes with safety and performance concerns caused by electromagnetic interaction of cables with the MRI system. As the number of in-bore devices increases, cabling also becomes a problem in terms of workflow.

Wireless powering promises to solve these issues generically. The default implementation of wireless power is by battery, most commonly by rechargeable lithium-ion batteries, which offer particularly high energy density. However, lithium-ion batteries tend to be magnetic due to cobalt, nickel, manganese, or iron content in their cathodes,⁴ precluding use close to or within the field of view in MRI. Inductive power transfer avoids this problem and has been shown to deliver impressive amounts of power.^{5,6} However, it requires dedicated transmission hardware integrated in the MRI system and incurs increased power deposition in the subject as well as potential interference with MR detection.

This is an open access article under the terms of the [Creative Commons Attribution-NonCommercial-NoDerivs](https://creativecommons.org/licenses/by-nc-nd/4.0/) License, which permits use and distribution in any medium, provided the original work is properly cited, the use is non-commercial and no modifications or adaptations are made.

© 2024 The Authors. *Magnetic Resonance in Medicine* published by Wiley Periodicals LLC on behalf of International Society for Magnetic Resonance in Medicine.

As an alternative, it has been suggested to harvest energy from the powerful radiofrequency (RF) pulses involved in MRI in the first place.^{7–10} Equally wireless, this completely parasitic approach avoids the need for additional power transmission and the hardware involved. It has been reported to harvest average power in the order of 100 mW from standard medical imaging sequences, using receiver form factors of just a few centimeters.¹⁰ However, tapping into the excitation RF field, also referred to as B_1 , alters that field and thus its effect on spin dynamics.^{7,9,10} B_1 perturbations near a harvester alter flip angles, causing artefacts in resulting images. Beyond artefacts, change in B_1 also alters local RF power deposition in the tissue (SAR), which is, again, a safety concern.

The goal of the present work is to solve this issue and render RF harvesting a fully viable option for the powering of on-body devices. We propose a strategy of selective shielding that suppresses B_1 perturbation by an on-body harvester while being transparent to B_1 itself. In addition, the harvester system is laid out to not perturb static and gradient fields, rendering it entirely stealthy to both the MRI system and the viewer of resulting images. In a 3T whole-body imager, we demonstrate that this approach permits concurrent on-body RF harvesting and MR imaging without significant artifacts.

2 | METHODS

2.1 | Selective shielding

For inductive RF energy harvesting, a receiving coil must couple to the B_1 field of the scanner. In the present work,

harvester coils are designed to sit on the subject's body, similar to surface coils for imaging but with the coil upright. The benefit of upright orientation is antisymmetry of the magnetic field of such coils in the adjacent plane tangential to the body, a property later exploited for selective shielding.

The electromagnetic behavior of harvester setups is determined by three-dimensional full-wave modeling using CST Microwave Studio.¹¹ In the model calculations, one or multiple harvester coils of given geometry are exposed to circularly polarized B_1 field. Currents induced in the coils produce secondary magnetic field, causing the B_1 distortions to be addressed (Figure 1A).

A naive approach to limiting this effect could be to introduce a conductive sheet underneath the harvester to act as a shield (Figure 1B). Field produced by the harvester would then be kept out of the body by eddy currents that it drives in the shield. This kind of approach, however, fails because a conductive sheet does not discriminate between fields originating from the harvester coil and the B_1 field generated by the scanner's transmit coil. The B_1 field will equally induce eddy currents in the sheet and thus be canceled in the body as illustrated in Figure 1B.

To prevent field perturbation both by the harvester and by the shield we employ a shielding strategy that selectively admits eddy currents driven by the harvester while blocking induction by the B_1 field, similar to previous efforts to decouple RF and gradient coils.¹² To create such a shield, we need to find a pattern of conductors that fully supports induction by the harvester while being inductively decoupled from the primary B_1 field. This is achieved as follows:

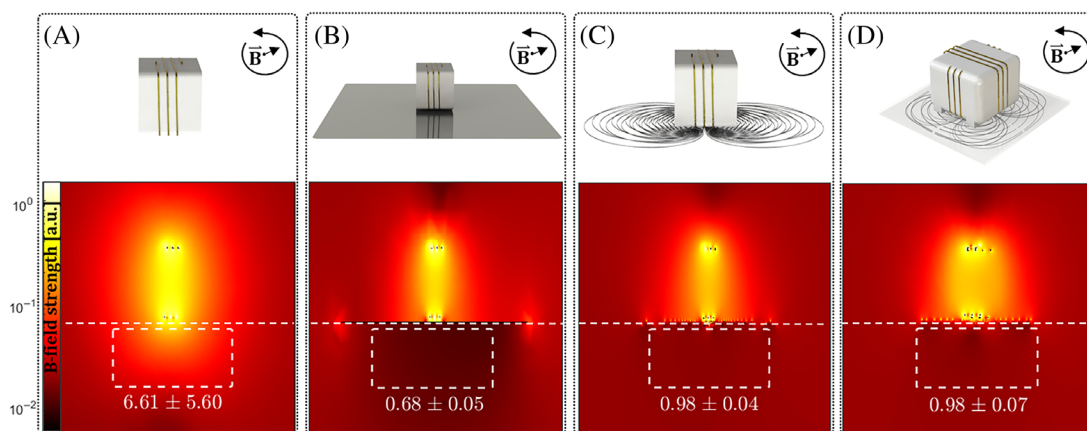


FIGURE 1 Simulations of the field around a coil driven by a circularly polarized B_1 field when (A) not shielded; (B) shielded with a perfectly conducting sheet; (C) shielded with a selective shield of 40 conductor traces. (D) is a simulation of two coils in quadrature configuration shielded with selective shields of seven conductor traces—the cross section is diagonal this time to include field produced by both coils. The horizontal line outlines the lower extent of the shield. The boxes outline an area in which the mean and SD of B_1 are analyzed. The values indicated are relative to the nominal B_1 value which corresponds to a mean of 1.

The currents that the harvester produces in an ideal, fully metallic shield are modelled through simulation and a set of discrete conductor loops are outlined along the resulting current paths. For best shielding performance, a large number of individual loops should be used, Figure 1C, while it however in practice is necessary to use a smaller number due to manufacturing complexity, Figure 1D. Coupling to the primary B_1 field is suppressed by exploiting the antisymmetry of the harvester field in conjunction with the uniformity of B_1 . Symmetric pairs of shield loops are connected to form figure-eight shapes, canceling induction by B_1 . The antisymmetry of the harvester field ensures that the figure-eight loops have shielding effect equivalent to that of the underlying pairs of individual loops.

One remaining issue is that of the scanner's gradient fields, which do not have the same homogeneous properties as B_1 . Due to this they cannot be decoupled in the same spatial manner. However, gradient induction can instead be blocked by filtering in the temporal domain as it occurs in a different frequency range.

Volume transmitters in MRI usually generate circularly polarized RF field. However, a single receiver coil is sensitive to only one linear polarization and thus highly orientation-dependent. At best, a single coil captures half of the available power while, with the worst orientation, it couples to neither mode of the transmitter. To address this problem, the system is fitted with two perpendicular harvester coils, forming a quadrature pair. This ensures that even with worst-case orientation, at least one linear B_1 polarization is fully captured.⁹ With optimal orientation (shield plane normal to z), the quadrature pair captures the circularly polarized field fully. Its efficiency thus varies between 0.5 and 1.0 rather than between 0 and 0.5 for a single coil. So, with quadrature harvesting, the power yield remains orientation-dependent, but at a higher orientation-average and it never drops below half of its optimum.

From the shielding point of view, this extension implies the addition of a second, perpendicular shield for the second coil. Due to geometry, each coil couples only to its own shield. The quadrature harvester and an illustration of the selective shielding concept are shown in Figures 1D and 2.

2.2 | Shield design

Designing a selective shield for the harvesting coil is done by taking the following steps: Given a desired coil geometry, a perfectly conducting plane is placed directly underneath the coil in the simulation model. The extent of the plane should be significantly larger than that of the coil

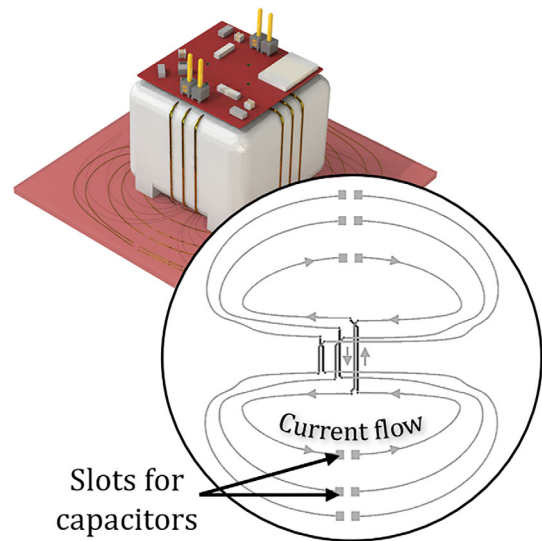


FIGURE 2 Rendering of the quadrature harvester with its selective shields and rectification circuitry. The inset is a detailed illustration of one of the shields.

itself such that little field from the coil reaches around the shield to the other side. The coil is driven by a current source connected to its two leads at the Larmor frequency, with no external (B_1) field present. The currents induced in the metallic plane are exported in the form of a vector field for postprocessing using custom software. From the exported data, a set of curves that fulfill the following condition are computed:

$$\frac{d\mathbf{x}_s(s)}{ds} \times \mathbf{J}(\mathbf{x}_s) = 0, \quad (1)$$

$\mathbf{x}_s(s)$ being such a curve and $\mathbf{J}(\mathbf{x}_s)$ the simulated current density. This type of curve is commonly referred to as a streamline. The streamlines outline how the currents need to flow to produce the desired shielding effect and are as such the templates for the shield conductors. The number of individual conductors should ideally be large and they should as such be as thin and as tightly spaced as possible. However, to limit ESR, parasitic capacitance, and manufacturing challenges it is necessary to settle with some intermediate conductor width and spacing. In the present work, the number of double-loops (figure-eight pairs) was set to 7, on a support twice as wide as the diameter of the harvester coil. With these choices, field leakage around the shield is similar to field leakage directly underneath the shield (Figure 1D). The calculated geometry is imported back into the simulation to confirm the shield's functionality before moving on with manufacturing. Once its functionality is confirmed, the geometry can be imported into a PCB design software for creating production files.

2.3 | Shield and receive coil implementation

The final shield is manufactured as a $60 \times 60 \text{ mm}^2$ three-layer circuit board. A simple two-layer board cannot be used due to the many interconnections of the figure-eight loops. A set of two capacitors of 100 pF are soldered to each loop for the purpose of high-pass filtering the gradient switching. Note that the loops are not resonant at the Larmor frequency, but rather at a frequency much lower, at about 50 MHz. This ensures that the capacitors impose relatively small impedances at the relevant frequency which allows for the necessary shield currents to flow while at the same time effectively causing an open circuit at the much lower gradient switching frequencies.

The receive coil is wound with a 0.5 mm wire and has a rectangular cross section of $20 \times 30 \text{ mm}^2$ and a self inductance of about 450 nH. Its windings sit on a three-dimensional printed body with grooves for the wire to ensure the correct geometry which is essential as its shield is designed for this specific coil. The overall design procedure can however be reapplied for a coil of any size and shape. To achieve the circularly polarized harvesting, a second coil is wound on the same three-dimensional printed body at a 90 degree offset and a second shield is sandwiched underneath the first one.

In the bottom row of Figure 1, the coil is exposed to a circularly polarized magnetic field similar to that in an MR scanner, with and without its selective shield, and the corresponding field perturbations are recorded.

2.4 | Harvesting circuitry

The leads of the receive coil are connected to a common rectification circuit via a matching network (Figure 3).¹³ A full bridge rectifier based on Schottky diodes is employed

for RF to DC conversion. The choice of Schottky diodes is fitting due to their low forward voltage drop which is valuable when rectifying signals with relatively small voltages. For the given coil geometry we would not expect EMFs higher than about 10 V in the scanner. At the output of the rectification stages a relatively large capacitor helps producing a steadier output DC signal and acts as a short-term power buffer during RF-free periods. The two rectifiers of the quadrature harvester feed into the same capacitor in parallel. Alternatively, the rectifier outputs could be connected to two series capacitors when more output voltage is desired. The size of the capacitor is in the order of a few mF—choosing the size of this capacitor is a compromise between higher DC voltages and a larger energy buffer. A matching network is necessary for maximizing power transferred from the coil to the rectification circuit and was modeled through simulations and ultimately tuned using a bench measurement setup. All the components in the circuitry were tested to ensure that they did not exhibit relevant magnetic behavior, either by virtue of the material used or by their small mass.

2.5 | Test bench

For lab tests, a power amplifier and an open transmission line were used to expose the harvester to pulsed RF magnetic fields with a well-defined magnitude, Figure 4. To avoid interference caused by conductive cables, the harvester output power was measured using an LED in the rectifier load. By connecting a fiber optical cable to the LED and reading out the light intensity on the outside with a calibrated receiver, measurements of power, voltage and current could be made simultaneously without any metallic cables. Due to the nature of the LED, this measurement approach has a minimum detectable voltage level and further implies a nonlinear loading. For evaluation of the

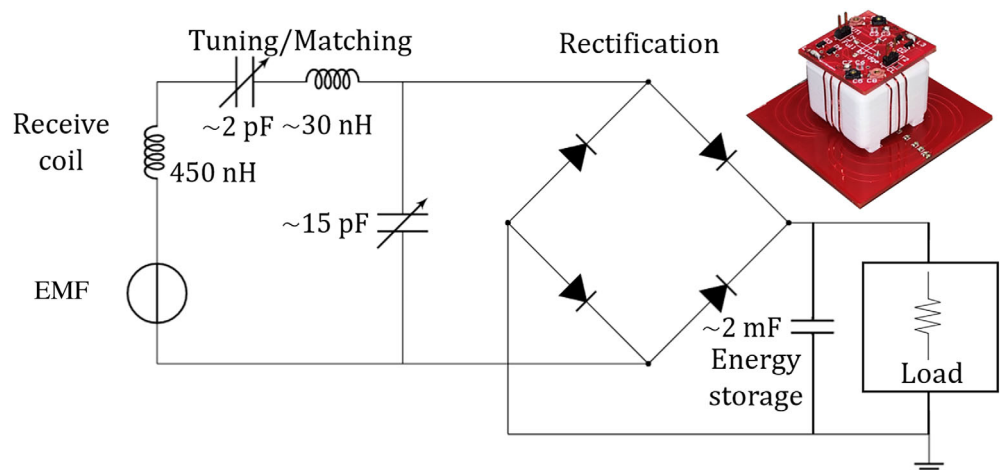


FIGURE 3 Schematic of the rectification circuit. The top right is a photograph of the realized harvesting system with its selective shields.

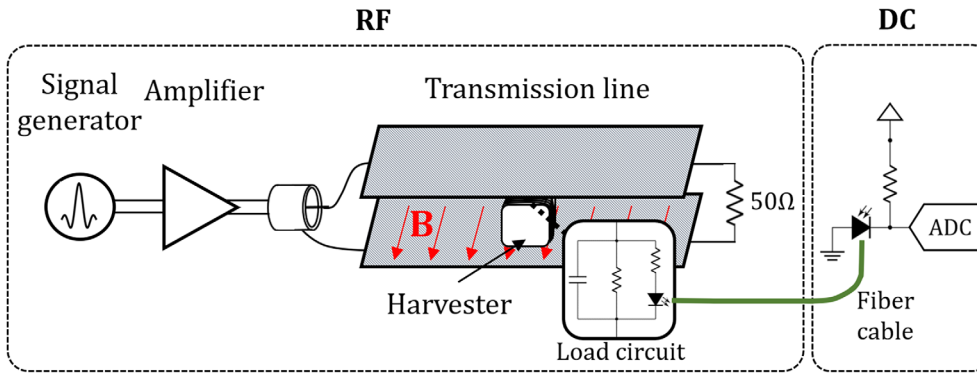


FIGURE 4 Test bench setup for exposing the harvesting system to radiofrequency fields. The optical power measurement circuit is detailed on the right-hand side.

rectifier performance, the said setup was used to measure its efficiency, which we define as

$$\eta = \frac{P_{\text{measured}}}{P_{\text{theoretical}}}, \quad (2)$$

where the theoretical maximum power delivered to a useful load can be derived from the maximum power transfer theorem,

$$P_{\text{theoretical}} = \frac{V^2}{4R}, \quad (3)$$

where V is the induced voltage and R the equivalent series resistance of the receiver coil at 128 MHz. Since aligning the receive coil perfectly against the magnetic field may be prone to errors, the alignment and measurement was performed multiple times.

The same setup was also used to measure the tuning and bandwidth of the rectifier by sweeping the RF frequency. Such measurements were facilitated through automated testing, where the signal generator frequency was controlled programmatically. An illustration of the bench setup can be found in Figure 4.

2.6 | Scanner setup

For in-bore evaluation of the harvester and shield, a water-based phantom was imaged with a gradient echo sequence on a Philips Ingenia 3T scanner (Figure 5). The sequence parameters used were $TR = 111$ ms, $TE = 4.4$ ms, $\alpha = 90^\circ$, a slice thickness of 4 mm and a maximum RMS B_1+ of $2.2 \mu\text{T}$. The scanner in question can output peak RF fields of $13 \mu\text{T}$. For highlighting the stealthy properties of the selective shield, the shield itself was imaged present on the phantom and was compared with a copper sheet of the same size. Further, the harvester was placed on the phantom and imaged without any shielding, with the copper sheet and finally with the selective shield. In the relevant cases, output power was measured concurrently

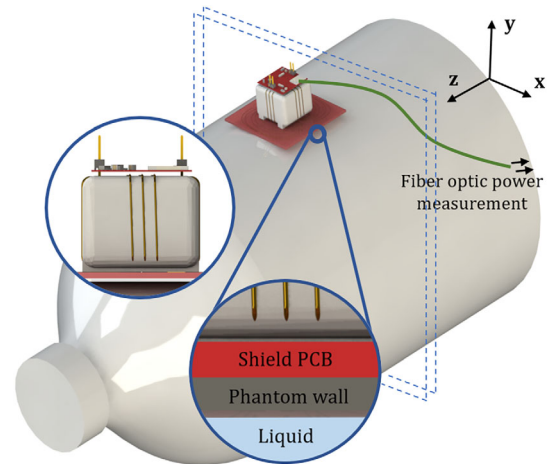


FIGURE 5 Imaging setup with the harvester on the phantom bottle.

with the imaging using the fiber optical setup. Note that the transmission line used previously is not relevant for measurements in the scanner.

Due to the output power being heavily dependent on the choice of imaging parameters and sequence, a set of common clinical sequences were played out and the respective powers delivered to the harvester load were recorded over time. The sequences used were gradient echo, spin echo, FLAIR, inversion recovery and turbo spin echo, all imaging in multislice mode.

3 | RESULTS

The simulation results displayed in the bottom row of Figure 1 are showcasing the way the selective shield can suppress field perturbations caused by the harvester. An ideal shield should not affect the B_1 field in the region of interest which is here used as a figure of merit to evaluate shielding performance. In Figure 1A, the field from the unshielded coil is displayed and a significant

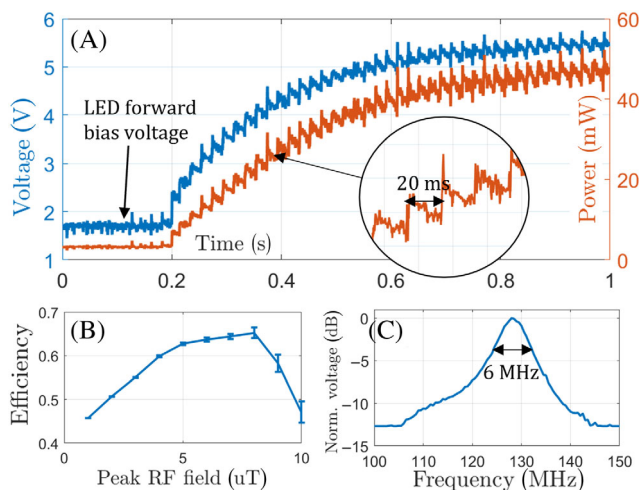


FIGURE 6 Harvester bench measurements. (A) Voltage and power when exposing the harvester to radiofrequency (RF) pulsing. The pulsing is turned on at 200 ms. (B) and (C) are measurements of efficiency and frequency dependency.

amplification of the excitation B1 field in the region of interest is observed, in line with observations reported by other authors. In Figure 1B where a fully metallic shield is applied there is instead a significant reduction in field due to eddy currents. At the edges of the metallic shield, fringe fields can be observed. In (C) a selective shield with a large set of shield conductors successfully suppresses the field perturbation caused by the harvester coil, maintaining the background field strength very close to its nominal value within the region of interest. Figure 1D shows how the background field can be kept very close to nominal values for a circularly polarized harvester and a shield with a much smaller number of shield conductors. A certain level of uneven field is observed directly underneath the shield which is due to the coarser set of shield conductors.

Figure 6A shows results captured on the test bench setup where a pulsed 128 MHz field of $2 \mu\text{T}$ was applied while reading out voltage and power. Once an equilibrium between the charging and discharging of the output capacitor is reached, the output settles at a more or less constant voltage and power output delivered to the load. The rectifier load including the LED settles at a stationary value of about 630Ω , corresponding to a voltage and power output of 5.5 V and 48 mW, respectively. The lower bound of the measurement due to the LED forward biasing voltage is visible at about 1.7 V and the RF pulse repetition rate can be clearly distinguished in the measurement from 200 ms onwards. Some noise is introduced into the measurement due to the nature of the photodiode used to receive the optical signal.

In Figure 6B the measurement of efficiency versus source field is displayed. The initial increase in efficiency can be explained with the higher induced voltage that comes with higher field strength, making the more or less constant diode voltage drop have less significance for the overall efficiency. The sharp decrease that follows can be explained by the diodes' breakdown voltage being reached. This agrees well with the general behavior reported for other RF harvesting circuits.¹³ In Figure 6C the frequency is swept from 100 to 150 MHz at a fixed $5 \mu\text{T}$ and a -3 dB bandwidth of about 6 MHz is observed at a center frequency of 128 MHz.

Figure 7 shows the results of the in-bore experiments made with the various harvester and shield configurations. The top right corner of Figure 7 displays power delivered to the load while taking images (D)–(G), which in each case amounts to about 60 mW throughout the imaging sequence. Figure 7A is a reference image of the phantom bottle, followed by (B) and (C) in which we introduce the full copper and the selective shield, omitting the harvesting circuitry. The results in these images agree well with predictions, where the fully metallic shield causes image artifacts due to eddy currents while the selective shield remains transparent to the scanner RF and is not visible in the images. The fringe fields predicted in Figure 1B can be observed around the edges of the shield in Figure 7B and the simulated field pattern underneath the metallic shield is also reflected in the image. In the second row of Figure 7 we introduce the harvester and the various types of shielding. In (D) we image the harvester without any shielding device and cause a large artefact directly underneath the receiver coil, as would be expected based on the predictions made in Figure 1A. Adding the fully metallic shield, (E), the artifact is virtually identical to that in (B), further suggesting that this shield does indeed prevent the field perturbations caused by the harvester but suffers from eddy currents that stem directly from the scanner B_1 . Finally, adding the selective shield underneath the harvester, (F) and (G), we observe a great reduction in the artifacts caused by the harvester with no notable deviations from the reference image visible to the naked eye.

In Figure 8 we show the DC power delivered to the harvester load for the set of imaging sequences. The specific implementations of the various sequences deliver a varying set of power outputs, reflecting more, or less, frequent RF pulsing. The average delivered power ranges from about 30 mW to 120 mW. Individual excitation, refocusing and inversion pulses can be identified in the different types of sequences.

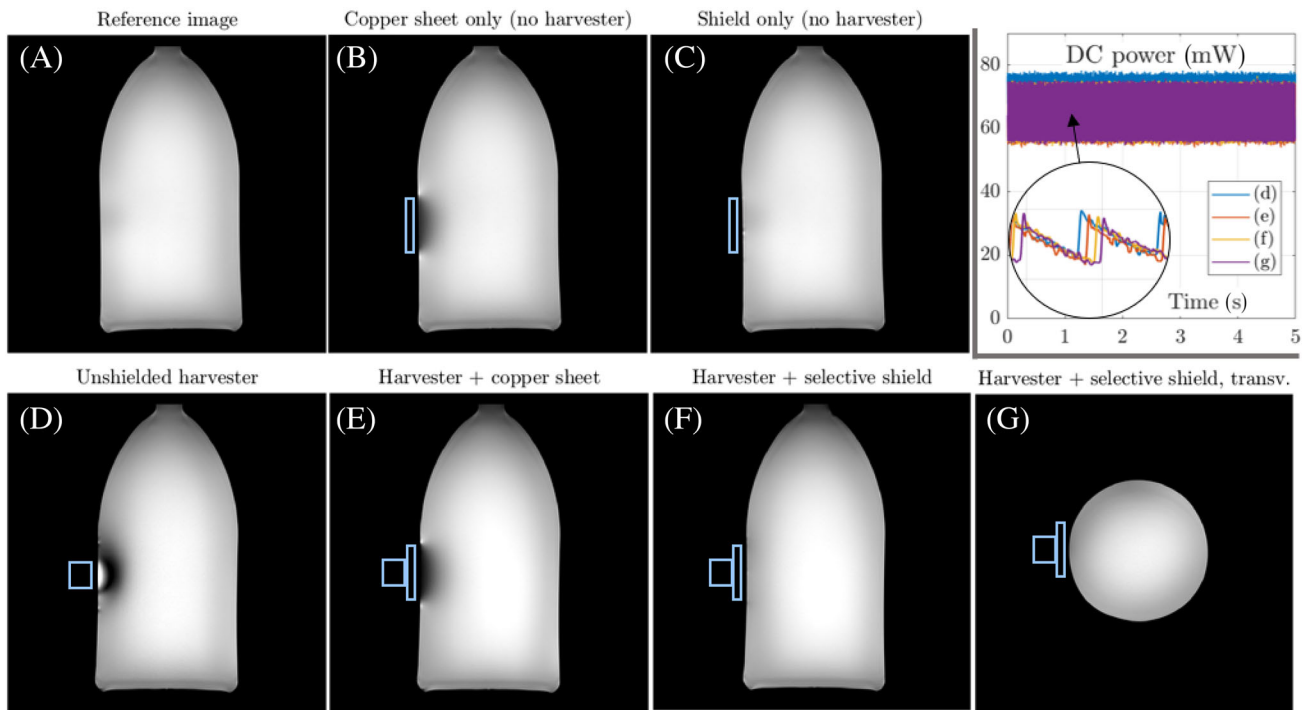


FIGURE 7 Phantom magnitude images. (A) Phantom only; (B) Copper sheet only; (C) Selective shield only; (D) Harvester, no shield; (E) Harvester and copper sheet; (F,G) Harvester and selective shield. All images share the same linear color scale. The top right inset displays power output measured during imaging.

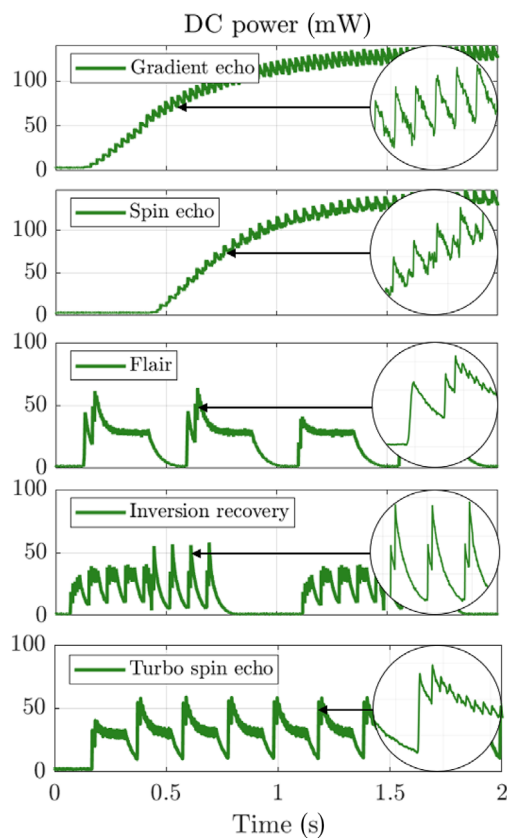


FIGURE 8 Harvested power output during a selection of standard imaging sequences.

4 | DISCUSSION AND CONCLUSION

In this paper we propose the concept of selective shielding for RF harvesting in MRI. With this we demonstrate the ability to perform stealthy RF harvesting in MRI for near-body applications, without depending on dedicated energy transmitters and while keeping imaging artifacts and change in SAR at very limited levels. The stealth property of the harvester relies not only to RF transparency but also to its gradient- and static field transparency as well as small size. We show that it is possible to deliver power to a DC load in the order of 60 mW from an MR scanner running a routine imaging sequence, while keeping the harvesting system virtually invisible.

To the MRI system, the harvester appears merely as a slight increase in RF load, which it automatically compensates for upon initial power calibration. Absorbed by the harvester, the added power does not by itself alter the tissue SAR. However, it will lead the power-based SAR calculation to slightly overestimate power deposition in tissue, adding to the RF safety margin. This effect will be very small though, considering that, at the SAR limit of 4 W/kg, 100 mW as harvested here correspond just only 25 g of tissue. SAR estimation based on B_1 in tissue should not be affected.

The previously established issue with RF harvesters in MRI is rather related to excessive field generation around the harvester receive coil which in turn leads to an uncertain choice of flip angle in the imaging as well as amplified local SAR. This effect can be observed in both the simulation and the imaging results presented in this paper.

The results show that shielding of a harvester coil can be achieved both by means of a fully metallic shield as well as a selective shield, but that only the selective shield suitably handles eddy currents. A selective shield eliminates the issues with eddy currents under certain conditions: The selective shield strictly needs to maintain its geometrical relationship with the harvester receive coil to remain functional. The selective shielding mechanism further depends on the homogeneity of the scanner's B_1 field and can as such only be used with transmit coils much larger than the harvester itself, where the relative change in B_1 field across the shield is small. The requirement of field uniformity could potentially be circumvented by using a shield that connects galvanically to the main receive coil. This approach would mean that the shield would carry a current that is equal in each conductor and equal to that of the receiver coil independently of the applied field and could as such produce the shielding effect in a nonhomogenous field. However, the complexity of designing such a coil and shield led to the decision to rather rely on inductive coupling.

The shield size is subject to a trade-off between shielding performance and handling of the device. Perfect shielding according to theory would require infinite extent. However, good performance can be accomplished with fairly small footprints already. In this work, the diameter of the shield was approximately twice the harvester size. At this ratio, subtle field leakage around the shield was similar to short-range leakage through the gaps between the shield loops. Relative size in this range appears generally advisable but will be a matter of individual optimization subject to shielding requirements and the exact geometry of the harvester coil. The number and specifications of the shield traces equally require optimization, constrained by limitations and tolerances of manufacturing. While an ideal shield would have arbitrarily dense, mutually isolated conductor traces, a typical printed circuit board can only be etched with gaps and trace widths down to around 0.1 mm. This leads to a compromise with some finite number of conductor traces. The results reported here suggest that viable compromises can be reached that still offer fully adequate shielding performance. Care should be taken to ensure that all components used on the shield, and all the other circuitry, are non-ferromagnetic.

A single selective shield, shielding a single polarization receiver, can only be realized on a printed circuit board that has at least three layers due to the interconnections.

To reduce size and simplify the design and manufacturing effort, it is possible to design pairs of shields for quadrature harvesters in combined six-layer PCBs, as opposed to the three-layer doublets we have used in this work.

The key parameters concerning the harvester coil are the equivalent series resistance (ESR) and the expected electromotive force (EMF) which scales with the coil cross section and number of turns. These relate directly to the coil size as well as the power that can be delivered to the load. The receiver coil should keep a low equivalent ESR as the delivered power is inversely proportional to it, but at the same time the coil needs to have a large enough cross section to deliver a sufficient amount of EMF. Choosing a thick wire gauge can help toward keeping the ESR down. Other things to consider are ESR caused by proximity effect and self resonance of the coil which can both be mitigated by increasing the distance between the coil windings. The optimal coil size will ultimately depend on the application—we are in this work using a coil of $2 \times 3 \text{ cm}^2$, and while this may be sufficient for applications that require below 100 mW of power, applications that are more demanding could be accommodated with a larger receiver. However, there also exist lower power applications that can be driven with significantly smaller amounts of power, for example, a Bluetooth Low Energy chip can be powered in the lower range of tens of mW, suggesting that it may well be possible to use even smaller harvesters for certain applications.

Beyond the ESR and EMF provided by the receiver coil, the delivered power is only limited by the efficiency of the rectifier. Optimizing the rectification circuit for efficiency for a specific load size or for a certain input power level could further improve delivered power, possibly reaching beyond the results presented in Figure 6. The decline of the efficiency curve in Figure 6 suggests that we only benefit from more available RF field up to a certain point—to make the system compatible with even higher RF field strengths, it would be necessary to choose diodes with larger breakdown voltage limits. The spectrum of the received signals will fall within a narrow range, typically within hundreds of kHz, which is why the -3 dB bandwidth of several MHz presented in Figure 6 is expected to be more than sufficient to receive all spectral energy.

The MR images displayed in Figure 7 agree very well with the predictions and confirm the validity of the shielding approach. The similarities observed between simulations and MR images further suggest that the simulation models indeed are good predictors of the harvester and shield's electromagnetic behavior. In Figure 7D we observe an image artifact centered around the unshielded harvesting system that is in line with what other authors have observed.

In the power output plot in Figure 7 the power observed differs slightly in the different cases and is marginally higher in the unshielded case, (D). This could have a variety of explanations, such as the shield slightly loading the receive coil and increasing its ESR or causing slight detuning of the rectification circuit.

The power output curves in Figure 8 show a diverse set of output power waveforms. In (A) and (B) the waveforms are relatively flat, suggesting that there is potential to supply a steady stream of harvested RF power to a load throughout an imaging sequence. In Figure 8C–E the average power is noted to be lower than in the previous cases and some longer RF free periods can be observed, amounting to a zero instantaneous power output.

The power delivered to the DC load is naturally limited by the amount of available RF power in the sequence. Higher and steadier power levels are obtained with higher RMS B1 and RF duty cycle, respectively. Due to the non-linear nature of the rectification circuitry, high RMS may be less useful when it goes along with low duty cycle. In general, low TR, large flip angles, and large RF bandwidth or multi-band RF will provide more harvestable power. In cases where the available power is insufficient, a potential solution would be to exploit remaining SAR margin for off-resonance RF pulses that are dedicated for wireless power. The intermittency of the RF power is in the nature of any given MR sequence so that some fluctuation is always to be expected. This means that a certain amount of temporary power buffer is necessary, for example in the form of a large capacitor. For the same reason, some kind of power management circuitry¹⁴ is likely necessary to accommodate swings in harvester output voltage. Such a power management circuit could be a conventional DC/DC converter. In the case of excess power a low-dropout regulator could also serve this purpose. As an alternative to conventional DC/DC converters, which typically have poor EMI characteristics and often use magnetic components, DC/DC conversion using switched capacitor converters has also been suggested.¹⁵

An artefact-free wireless power source has potential particularly for on-body applications: Power levels around 100 mW as achieved here have potential, e.g., for powering sensors such as oximeters, respiration sensors, ECG, EEG, as well as motion tracking sensors and potentially NMR field probes.^{16–22} The concept of powering entire MR receive chains is an attractive prospect and could perhaps be considered the ultimate challenge for wireless power in MRI. With the results presented in this work, this is not quite within reach, with a typical single receive chain requiring power levels in the order of several hundreds of mW.^{23,24} However, if increasing the overall system size is permissible, the achievable power levels could possibly come within reach of powering an entire receive chain.

The fundamental incentive for RF harvesting is to allow for wireless devices—this implies that there must also be wireless communication of some sort. RF harvesting could also be used to power communication hardware such as Bluetooth Low Energy²⁵ or other forms of in-bore wireless communication²⁶ and a target application could as such be made wireless in a two-fold sense, with both power and data being transmitted over the air.


ACKNOWLEDGMENTS

The authors would like to thank Thomas Schmid for his valuable input on electromagnetic shielding. Open access funding provided by Eidgenossische Technische Hochschule Zurich.

CONFLICT OF INTEREST STATEMENT

The authors declare no potential conflict of interests.

ORCID

Oskar Bjorkqvist  <https://orcid.org/0009-0001-1918-8176>

Klaas P. Pruessmann  <https://orcid.org/0000-0003-0009-8362>

REFERENCES

1. Van Niekerk A, Meintjes E, Van der Kouwe A. A wireless radio frequency triggered acquisition device (WRAD) for self-synchronised measurements of the rate of change of the MRI gradient vector field for motion tracking. *IEEE Trans Med Imaging*. 2019;38:1610-1621.
2. Pancoast L, Brantner D, Wiggins R, Walczyk J, Brown R. Wireless body sensor data acquisition platform for motion tracking. Paper presented at: ISMRM. 2021.
3. Wei J, Liu Z, Chai Z, Yuan J, Lian J, Shen GX. A realization of digital wireless transmission for MRI signals based on 802.11 b. *J Magn Reson*. 2007;186:358-363.
4. Li M, Lu J. Cobalt in lithium-ion batteries. *Science*. 2020;367:979-980.
5. Byron K, Robb F, Stang P, Vasanaawala S, Pauly J, Scott G. An RF-gated wireless power transfer system for wireless MRI receive arrays. *Concepts Magn Reson Pt B Magn Reson Eng*. 2017;47B:e21360.
6. Byron K, Winkler SA, Robb F, Vasanaawala S, Pauly J, Scott G. An MRI compatible RF MEMs controlled wireless power transfer system. *IEEE Trans Microwave Theory Tech*. 2019;67:1717-1726.
7. Kelly B, Robb F, Vasanaawala S, Pauly J, Scott G. Harvesting power wirelessly from MRI scanners. Paper presented at: Proceedings of the International Society for Magnetic Resonance in Medicine. vol. 1535. 2019; Montreal, Canada.
8. Ganti A, Wynn T, Lin J. A novel energy harvesting circuit for RF surface coils in the MRI system. *IEEE Trans Biomed Circuit Syst*. 2021;15:791-801.
9. Seregin PS, Burmistrov OI, Solomakha GA, Kretov EI, Olekhno NA, Slobozhanyuk AP. Energy-harvesting coil for circularly polarized fields in magnetic resonance imaging. *Phys Rev Appl*. 2022;17:044014.

10. Venkateswaran M, Kurpad K, Brown JE, Fain S, Weide D. Wireless power harvesting during MRI. Paper presented at: 2020 42nd Annual International Conference of the IEEE Engineering in Medicine & Biology Society (EMBC) IEEE. 2020:1469-1472.
11. CST Microwave studio. <https://www.3ds.com/products-services/simulia/products/cst-studio-suit>
12. Bidinosti CP, Hayden ME. Selective passive shielding and the faraday bracelet. *Appl Phys Lett*. 2008;93:174102.
13. Valenta CR, Durgin GD. Harvesting wireless power: survey of energy-harvester conversion efficiency in far-field, wireless power transfer systems. *IEEE Microwave Magazine*. 2014;15:108-120.
14. Martins GC, Serdijn WA. An RF energy harvesting and power management unit operating over- 24 to+ 15 dBm input range. *IEEE Trans Circuit Syst I Regul Papers*. 2020;68:1342-1353.
15. Schildknecht CM, Brunner DO, Pruessmann KP. In-bore voltage inversion with very low EMI by a switched capacitor converter. Paper presented at: ISMRM. 2020.
16. De Zanche N, Barmet C, Nordmeyer-Massner JA, Pruessmann KP. NMR probes for measuring magnetic fields and field dynamics in MR systems. *Magn Reson Med*. 2008;60:176-186.
17. Ooi MB, Krueger S, Thomas WJ, Swaminathan SV, Brown TR. Prospective real-time correction for arbitrary head motion using active markers. *Magn Reson Med*. 2009;62:943-954.
18. Haeberlin M, Kasper L, Barmet C, et al. Real-time motion correction using gradient tones and head-mounted NMR field probes. *Magn Reson Med*. 2015;74:647-660.
19. Gross S, Barmet C, Dietrich BE, Brunner DO, Schmid T, Pruessmann KP. Dynamic nuclear magnetic resonance field sensing with part-per-trillion resolution. *Nat Commun*. 2016;7:13702.
20. Aranovitch A, Haeberlin M, Gross S, et al. Prospective motion correction with NMR markers using only native sequence elements. *Magn Reson Med*. 2018;79:2046-2056.
21. Eschelbach M, Aghaeifar A, Bause J, et al. Comparison of prospective head motion correction with NMR field probes and an optical tracking system. *Magn Reson Med*. 2019;81:719-729.
22. Mandal R, Babaria N, Cao J, Liu Z. Adaptive and wireless recordings of electrophysiological signals during concurrent magnetic resonance imaging. *IEEE Trans Biomed Eng*. 2019;66:1649-1657.
23. Sporrer B, Wu L, Bettini L, et al. A fully integrated dual-channel on-coil CMOS receiver for array coils in 1.5–10.5 T MRI. *IEEE Trans Biomed Circuit Syst*. 2017;11:1245-1255.
24. Port A, Reber J, Vogt C, et al. Towards wearable MR detection: a stretchable wrist array with on-body digitization. Paper presented at: *Proceedings of International Society of Magnetic Resonance in Medicine*. 2018:17.
25. Vogt C, Reber J, Waltisberg D, et al. A wearable bluetooth LE sensor for patient monitoring during MRI scans. Paper presented at: 2016 38th Annual International Conference of the IEEE Engineering in Medicine and Biology Society (EMBC). IEEE. 2016; Orlando, USA:4975-4978.
26. Aggarwal K, Joshi KR, Rajavi Y, et al. A millimeter-wave digital link for wireless MRI. *IEEE Trans Med Imaging*. 2017;36:574-583.

How to cite this article: Bjorkqvist O, Pruessmann KP. Stealth RF energy harvesting in MRI using selective shielding. *Magn Reson Med*. 2024;92:406-415. doi: 10.1002/mrm.30048